

OPTIMIZED SIZE-ADAPTIVE FEATURE EXTRACTION BASED ON CONTENT-MATCHED RATIONAL WAVELET FILTERS

Tan-Toan Le[†], Mathias Ziebarth[‡], Thomas Greiner[†], Michael Heizmann[§]

[†] Pforzheim University, Institute for Applied Research, Tiefenbronnerstr. 65, 75175 Pforzheim, Germany

[‡] Karlsruhe Institute of Technology, Institute for Anthropomatics, Adenauerring 4, 76131 Karlsruhe, Germany

[§] Fraunhofer IOSB, Fraunhoferstr. 1, 76131 Karlsruhe, Germany

ABSTRACT

One of the challenges of feature extraction in image processing is caused by the fact that objects originating from a feature class don't always appear in a unique size, and the feature sizes are diverse. Hence, a multiresolution analysis using wavelets should be suitable. Because of their integer scaling factors classical dyadic or M -channel wavelet filter banks often don't match very well the corresponding feature sizes occurring within the image. This paper presents a new method to optimally extract features in different sizes by designing a rational biorthogonal wavelet filter bank, which matches both the features' characteristics and the significant sizes of the most dominant features' sizes. This is achieved by matching the rational downsampling factor to the different feature sizes and matching the filter coefficients to the feature characteristics. The presented method is evaluated with the detection of defects on specular surfaces and of contaminations on manufactured metal surfaces.

Index Terms— Wavelet transform, Feature matched filters, Classification, Machine Vision

1. INTRODUCTION

In recent years feature extraction based on wavelet methods has been increasingly used in different research and application fields. Jahankhani et al. [1] used a discrete wavelet transform with *Daubechies-wavelets* to extract features from electroencephalogram (EEG) signals and classified them by means of neural networks. Based on the *Morlet-wavelet* a denoising method was applied to feature extraction for mechanical vibration signals in [2]. For feature extraction from near-infrared data Mallet et al. [3] optimized the wavelet filter coefficients by maximizing a chosen discriminant criterion between classes with respect to conditions for orthogonality and regularity of filters. Besides optimizing the wavelet as a specific wavelet filter bank, another improvement to enhance the performance of feature extraction is to design the wavelet filter bank so that it can match features in not just only coefficients but also various sizes. However, the application of standard dyadic or M -channel wavelet filter banks has the

drawback, that the dilation factors are always integer values, which leads to inflexibility when scaling is applied. In this paper a new approach for feature extraction based on matching wavelet filters to feature characteristics is proposed. The wavelet filter banks are constructed to be biorthogonal to have more degrees of freedom during filter design. To demonstrate how the presented method works, the designed wavelet filter banks are evaluated using detection tasks for defects on specular surfaces as well as for contaminations on manufactured metal surfaces.

The optimization algorithm takes place in two steps: i) determining the dominant feature's sizes and selecting the most suitable rational scaling factors with respect to these sizes and ii) matching the filter coefficients of the wavelet filter bank to selected image features.

The paper is organized as follows: the two steps of the optimization method are presented in Section 2 and 3 respectively. In Section 4 applications of the new method for classifying data from deflectometric measurements as well as for detecting contaminations on metal surfaces are described. Finally a conclusion is made in Section 5.

2. MATCHING TO DOMINANT FEATURE SIZES

2.1. Determining dominant feature sizes

In the preparation step the image to be classified was first segmented by different conventional image processing algorithms, for example *Laplacian of Gaussian* or *Prewitt operator*, and then the feature sizes (also called as feature stretching) were measured. Based on the measured feature sizes by each segmentation algorithm a joint result was built. For each feature set consisting of features of the same class but different stretching, the most dominant feature sizes are chosen. The idea for size-adaptive feature extraction optimization is to design a wavelet filter bank with rational sampling factors, which matches the filter lengths to dominant feature sizes.

2.2. Rational wavelet filter bank

One of the first approaches for designing wavelet filter banks with rational sampling factors was introduced by Kovacevic and Vetterli [4]. After that, some new ideas were presented by other authors, for example in [5] or [6]. Among the methods for designing rational wavelet filter banks existing in the literature, the approach of Nguyen et al. [7] was chosen for this paper, because it can not only construct a biorthogonal wavelet filter bank but also allows a large choice of rational sampling factors. By this method a filter bank consisting of two filters \mathbf{h}_{LP} and \mathbf{h}_{HP} with respective subsampling factors (p_0/M) and (p_1/M) is created (Figure 1), with the restriction that $p_0 + p_1 \stackrel{!}{=} M$.

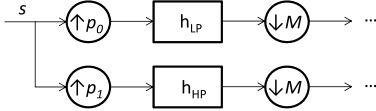


Fig. 1. Wavelet filter bank with rational sampling factor (p_0/M) and (p_1/M) .

As long as the z -Transform $H_{LP}(z)$ and $H_{HP}(z)$ of \mathbf{h}_{LP} and \mathbf{h}_{HP} can be decomposed into:

$$H_{LP}(z) = \sum_{n=0}^{p_0-1} z^{Mn} H_n(z^{p_0}) \quad \text{and} \quad (1)$$

$$H_{HP}(z) = \sum_{n=0}^{p_1-1} z^{Mn} H_{n+p_0}(z^{p_1}), \quad (2)$$

the given rational filter bank is equivalent to a filter bank with M channels: $H_0, H_1, \dots, H_{p_0+p_1-1}$. This means, that in this case the non-uniform filter bank with rational sub sampling factors (p_0/M) and (p_1/M) is equivalent to a uniform M -channel filter bank [7].

2.3. Matching scaling factors to feature sizes

First of all a set \mathcal{F} consisting of features of the same class but different sizes is created. As described above the goal of this feature extraction optimization is to design a biorthogonal wavelet filter bank as shown in Figure 1 with rational sampling factor (p_1/M) by filter \mathbf{h}_{HP} , which has a length of λ and a curve shape similar to the feature in \mathcal{F} . Based on the number n_{l_j} of defects with the feature size l_j , the t highest numbers, which means the t most dominant feature sizes in \mathcal{F} are chosen: $T = \{l_j, j = 0, \dots, t-1, l_j < l_{j+1}\}$. On the basis of T , p_1 , M and λ should be defined so that:

$$\frac{p_1}{M} \lambda \approx l_{t-1}, \dots, \left(\frac{p_1}{M}\right)^{u_1} \lambda \approx l_1, \left(\frac{p_1}{M}\right)^{u_0} \lambda \approx l_0. \quad (3)$$

It means, with the help of sampling factor (p_1/M) , the length λ of filter \mathbf{h}_{HP} is scaled to the size l_{t-1} by the first transformation and to other sizes after some transformations. For example sizes l_1, l_0 are obtained by the u_1 -th and the u_0 -th

transformation ($u_i \in \mathbb{N}, 1 < u_i < u_{i-1}$). Hence, the filter matches most of the dominant feature sizes after some transformations. One of the possible ways to find the most dominant sizes in \mathcal{F} is, for example, by means of a size histogram. After this step the sampling factors p_1 , M and consequently p_0 ($p_0 = M - p_1$) for the desired filter bank are found.

3. MATCHING TO FEATURE CHARACTERISTICS

3.1. Conditions for biorthogonality

As described in Section 2.2, as long as the conditions in (1) and (2) are fulfilled, a non-uniform filter bank with rational sub sampling factors (p_0/M) and (p_1/M) is equivalent to a uniform M -channel filter bank. An M -channel uniform filter bank consists of M analysis filters \mathbf{H}_t as well as M synthesis filters \mathbf{G}_t ($t = 0, \dots, M-1$). A signal $s(n)$ can be analyzed by the filters \mathbf{H}_t to create decomposition coefficients. With the filters \mathbf{G}_t these coefficients can be used to construct a signal $\hat{s}(n)$. In case of $s(n) = z^{-n_0} * \hat{s}(n)$ the filter bank is called a *filter bank allowing perfect reconstruction* [8]. Mathematically, the perfect reconstruction condition guarantees the biorthogonality of the filter bank. This condition is fulfilled, if the determinant $\Delta_Q(z)$ of the polyphase-matrix $Q(z)$ of the filters \mathbf{h}_t consists of only a single term z^{-n_0} [9]. $Q(z)$ has the form:

$$Q_{ij}(z) = z^{-j} H_{ij}(z^M). \quad (4)$$

Here $H_{ij}(z^M)$ is the j th polyphase component of the i th filter [8]. Its determinant $\Delta_Q(z)$ can be calculated as:

$$\Delta_Q(z) = c_0 z^{-M \frac{M-1}{2}} + \dots + c_{N-M} z^{-[MN-M \frac{M+1}{2}]}, \quad (5)$$

with the constants c_m , $m = 0, \dots, N-M$.

3.2. Matching filter coefficients to feature characteristics

For each class C_i on a given image I a one-dimensional curve to describe a characteristic feature is estimated. This curve is defined as the mean profile of the defect. After normalization, the N sampling points of the curve define a feature filter \mathbf{h}_F with length N . The typical feature curve \mathbf{h}_F is used for constructing a 2-channel biorthogonal wavelet filter bank. In the first step the filter \mathbf{h}_{LP} is optimized as a low pass with the least square objective function:

$$f_0(\mathbf{h}_{LP}) = \mathbf{h}_{LP}^T (\mathbf{P}_{P_0} + \mathbf{P}_{S_0}) \mathbf{h}_{LP}, \quad (6)$$

where \mathbf{P}_{P_0} and \mathbf{P}_{S_0} are real symmetric positive semi-definite matrices described in [10] to optimize the pass-band and stop-band of filter \mathbf{h}_{LP} . The objective function $f_0(\mathbf{h}_{LP})$ is to be minimized with the restriction:

$$g_0 : \|\mathbf{h}_{LP} - \mathbf{h}_F\|^2 > \epsilon_0. \quad (7)$$

This approach effects that the first filter \mathbf{h}_{LP} is constructed to be a low-pass filter and different from the given feature filter \mathbf{h}_F .

After the first step the filter coefficients of \mathbf{h}_{LP} are available for designing an appropriate biorthogonal wavelet filter \mathbf{h}_{HP} . Filters \mathbf{h}_{LP} and \mathbf{h}_{HP} build together vectors \mathbf{h}_i ($i = 0, \dots, M-1$) as polyphase components for given rational sampling factors (p_0/M) and (p_1/M) as in Figure 1:

$$\mathbf{h}_i[n] = \begin{cases} \mathbf{h}_{LP}[i + np_0] & \text{for } i = 0, \dots, p_0 - 1, \\ \mathbf{h}_{HP}[i - np_0 + np_1] & \text{for } i = p_0, \dots, M - 1. \end{cases} \quad (8)$$

As described in Section 2.2 the non-uniform filter bank (FB) of \mathbf{h}_{LP} , \mathbf{h}_{HP} with rational sampling factor (p_0/M) and (p_1/M) is now equivalent to a uniform M -channel FB of \mathbf{h}_i . The non-uniform FB is therefore biorthogonal and allows perfect reconstruction if the equivalent uniform FB has this property. Due to the condition for perfect reconstruction introduced in Section 3.1, all constants c_m in (5) except one need to be set to 0. c_m consist of coefficients of \mathbf{h}_i , which are also coefficients of \mathbf{h}_{LP} and \mathbf{h}_{HP} as in (8), and hence can be used as constraints for designing filter \mathbf{h}_{HP} .

Filter \mathbf{h}_{HP} is optimized by the least square objective function:

$$f_1(\mathbf{h}_{HP}) = \mathbf{h}_{HP}^T (\mathbf{P}_{P_1} + \mathbf{P}_{S_1}) \mathbf{h}_{HP}. \quad (9)$$

As in (6) \mathbf{P}_{P_1} and \mathbf{P}_{S_1} optimize here the pass-band and stop-band for \mathbf{h}_{HP} . Furthermore the distance between filter \mathbf{h}_{HP} and the given feature filter \mathbf{h}_F should be smaller than a given constant ϵ_1 , which also means \mathbf{h}_{HP} should be similar to \mathbf{h}_F :

$$g_1 : \|\mathbf{h}_{HP} - \mathbf{h}_F\|^2 < \epsilon_1. \quad (10)$$

The filter \mathbf{h}_{HP} can therefore be optimized by minimizing the function $f_1(\mathbf{h}_{HP})$ with the constraints $c_m \stackrel{!}{=} 0$ (for all c_m except one) and g_1 .

Applying the sampling factors p_0 , p_1 and M found in Section 2.3 the desired biorthogonal wavelet filter bank with rational sampling factors can be constructed and then used for analyzing data. All analysis results at k -th iteration with $(p_1/M)^k \lambda = l_j \in T$ are considered as features d_k for classification in the next step (T is the set of dominant sizes as defined before in Section 2.1).

4. APPLICATIONS

The introduced size-adaptive feature extraction was applied on different image processing tasks. In the first application the method was used for defect classification on specular surfaces obtained by deflectometry. In the second one it was used for detecting contaminations on manufactured metal surfaces.

4.1. Defect classification on specular surfaces

For examining highly reflective surfaces, deflectometric methods are most suitable because they exploit the specularity of the surface and feature a high sensitivity to geometric deviations from the ideal surface shape.

4.1.1. Fundamentals of deflectometry

A deflectometric measurement system consists of a camera with image plane I , a specular surface S and a screen L arranged in a triangular setup. On the screen sinus patterns in horizontal and vertical direction for phase shifting methods are displayed. The camera observes a distorted pattern of the screen over the specular surface. By observing a sequence of patterns, viewing rays from the camera plane P_I can be uniquely assigned to points on the screen P_L :

$$l : P_I \mapsto P_L, l[u, v] = (x_L, y_L). \quad (11)$$

This mapping l is called deflectometric registration. Without knowing the distance between the camera and the surface it is impossible to unambiguously reconstruct the surface from the deflectometric registration. An overview of several regularizing methods for deflectometry is given by Werling et al. [11]. In the following, we assume that a surface $S(m, n)$ is obtained as result of the deflectometric reconstruction in a $2\frac{1}{2}$ D representation¹:

$$S(m, n) = z, \text{ with } (m, n) \in \mathbb{N}^2, z \in \mathbb{R}. \quad (12)$$

In this case z is the estimated height of each pixel. While many different defects can appear on the surface, most of them have characteristic shapes. The size of the defects ranges from very small to large, but their shape remains the same for each class. For this reason wavelets can be considered as an appropriate method to detect and classify these defects.

4.1.2. Defect classification

In this paper a supervised segmentation is applied. For the classification a maximum a posteriori decision is made for each point on the surface separately. By defining the parameter vectors $\boldsymbol{\mu}_i$ and $\boldsymbol{\sigma}_i$ as mean and standard deviation of each coefficient in class C_i for all features d_k in vector \mathbf{d} , the probability for \mathbf{d} belonging to class C_i is determined by Bayes' rule:

$$p(\boldsymbol{\mu}_i, \boldsymbol{\sigma}_i | \mathbf{d}) = \frac{p(\mathbf{d} | \boldsymbol{\mu}_i, \boldsymbol{\sigma}_i) p(\boldsymbol{\mu}_i, \boldsymbol{\sigma}_i)}{p(\mathbf{d})}. \quad (13)$$

Like described in [12] coefficients can often be assumed as Laplace distributed. In consequence the likelihood for class C_i is modelled as product of univariate Laplace distributions:

$$p(\mathbf{d} | \boldsymbol{\mu}_i, \boldsymbol{\sigma}_i) = \prod_k \frac{1}{\sigma_{i,k} \sqrt{2}} \exp \left(-\sqrt{2} \frac{|d_k - \mu_{i,k}|}{\sigma_{i,k}} \right). \quad (14)$$

The parameters $\boldsymbol{\mu}_i$ and $\boldsymbol{\sigma}_i$ for each class C_i are learned with a training set for each class. The prior is chosen as being uniformly distributed, but this could be changed in practice in case that appropriate knowledge is available.

¹The notation $2\frac{1}{2}$ D denotes that for each point in a 2D domain, exactly one height value is available.

4.1.3. Results

Deflectometry data from different curved lacquered surfaces with several large dents and many small pimples were analyzed. Since dents and pimples are the most common defects on our lacquered surfaces, the experiment was performed using these two classes. There are totally 3 large dents and 33 pimples on the first surface, 3 large dents and 14 pimples on the second surface, and 123 pimples on the third surface to be detected. Additionally the surfaces have uneven formations, called orange peel, which results in a high measurement noise and complicates the detection of defects.

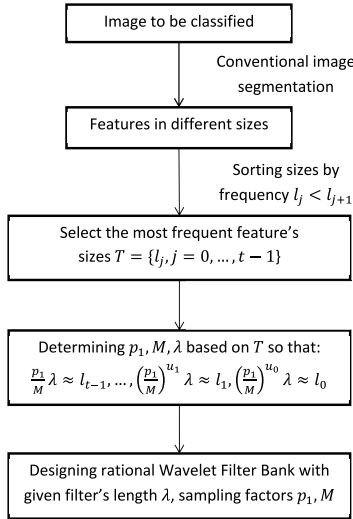


Fig. 2. Process for determining sampling factors

The process for determining scaling factors p_0 , p_1 and M describe in Section 2.3 is summarized in Figure 2. After segmentation and measurement with different conventional segmentation algorithms a joint result of the feature sizes (or so called feature stretching) for each class on the surface is built. Figure 3 shows the size histogram of the feature *pimple* on a surface. Based on this histogram the most dominant sizes of the features can be derived. In this example the 3 most common lengths: 6, 7 and 11 (defined as l_0 , l_1 and l_2 respectively) are chosen. By applying the calculation as described in 2.3, it can be found that $\lambda = 14$, $p_1 = 4$ and $M = 5$ satisfy $\frac{p_1}{M} \lambda \approx l_2$, $(\frac{p_1}{M})^3 \lambda \approx l_1$, $(\frac{p_1}{M})^4 \lambda \approx l_0$. Now, by means of the algorithm presented in 3.2 a filter bank with the rational sampling factor $(\frac{4}{5})$ consisting of a filter optimized for the defect pimple with length 14 together with its biorthogonal wavelet filter can be constructed. The impulse response of the original pimple filter and the filter obtained at the first transformation are shown in Figure 4. Obviously, the general shape of the pimple filter does not change after the transformation. The same results were also achieved for l_1 and l_2 .

By means of these filter banks, classifications for the two defect classes *pimple* (C_p) and *dent* (C_d) were made. The

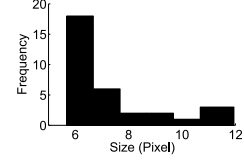


Fig. 3. Size histogram of the feature *pimple*.

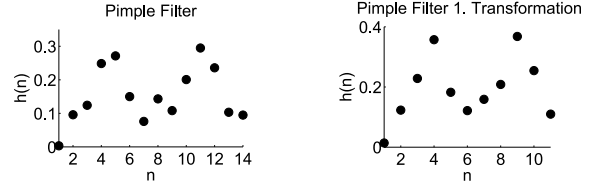


Fig. 4. Impulse response of pimple matched filter.

accuracy value was chosen as metric for classification:

$$Accuracy = \frac{\#TP + \#TN}{\#TP + \#FP + \#FN + \#TN}, \quad (15)$$

where $\#TP$, $\#TN$, $\#FP$ and $\#FN$ are the respective numbers of true positives, true negatives, false positives and false negatives. The obtained accuracy by applying the *rational biorthogonal wavelet filter bank (RWFB)* is presented in Table 1 with different numbers t of chosen dominant sizes. As reference *correlation filters*, standard wavelets filter bank as well as *M-channel optimized wavelet filter banks (MCFB)* introduced in [12] were also employed. The filter banks for *MCFB* were optimized to given defect classes, but in contrast to *RWFB* the scaling factors for *MCFB* were all integers.

It can be seen that with a larger number t of chosen dominant feature sizes, the classification with *RWFB* got better. With three considered sizes the *RWFB* provides better results than *MCFB* as well as the standard wavelet. Up to 89% of *pimple* as well as 95% of *dent* are classified correctly by *RWFB*. Due to the specific optimization to given defect classes the filter banks with *MCFB* and *RWFB* classify the surfaces better than the one with the standard wavelet. And by means of matching the filter lengths to dominant feature sizes in the image, the filter banks with *RWFB* deliver better results than the one with *MCFB*.

| | | Accuracy | |
|---------------------------------|--------------|----------|-------|
| Standard methods | | C_d | C_p |
| Correlation filters | | 60% | 66% |
| Biorthogonal spline wavelet 3.5 | | 88% | 35% |
| Method | Matched | C_d | C_p |
| <i>MCFB</i> | C_d | 90% | 73% |
| <i>MCFB</i> | C_p | 67% | 78% |
| <i>RWFB</i> | $C_p, t = 1$ | 75% | 70% |
| <i>RWFB</i> | $C_p, t = 2$ | 84% | 84% |
| <i>RWFB</i> | $C_p, t = 3$ | 95% | 89% |

Table 1. Comparison of the classification accuracy using different wavelet filter banks for our classification method with the classes *dent* C_d and *pimple* C_p .

| | | Accuracy |
|---------------------------------|--------------|----------|
| Thresholding | | 70% |
| Biorthogonal spline wavelet 3.5 | | 68% |
| <i>RWFB</i> | $C_s, t = 1$ | 94% |
| <i>RWFB</i> | $C_s, t = 2$ | 95% |
| <i>RWFB</i> | $C_s, t = 3$ | 96% |

Table 2. Accuracy using different wavelet filter banks for classification of the class *stain* C_s .

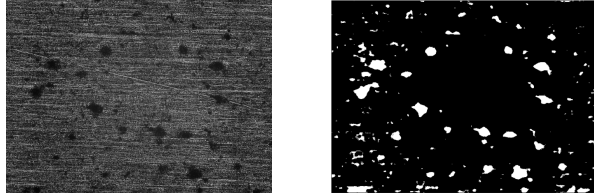


Fig. 5. Textured metal surface with contaminations (left) and detected contaminations (right).

4.2. Detection of contaminations on a metal surface

The feature extraction method was also used for a second application, where totally 78 contaminations in form of black stains on a metal surface should be detected. On the surface visible textures which are caused by manufacturing and which complicate the detection are present. In this case the brightness curve of a stain on the surface was considered as the feature characteristic. In Table 2 the accuracy by using *RWFB*, *Thresholding* and a filter bank with standard wavelet used for detection is shown. The detection rate of the class *stain* C_s is 94%, 95% and 96% by choosing 1, 2 and 3 dominant feature sizes, respectively, compared to 68% with the standard biorthogonal wavelet and 70% with *Thresholding*. Figure 5 shows the textured metal surface with black stains to be detected (left) and the result of stain detection on the surface (right).

5. CONCLUSION

In this paper a novel method for optimizing feature extraction based on content-matched rational biorthogonal wavelet filter banks was introduced. Based on i) matching the filter coefficients to feature characteristics and ii) matching the rational subsampling factors to dominant feature sizes the proposed method achieves better feature extraction and therefore better classification results than other approaches. The presented approach was evaluated by different image processing tasks: defect classification on specular surfaces examined by deflectometry and detection of contaminations on manufactured metal surfaces.

6. ACKNOWLEDGEMENT

This research work was financed by Baden-Württemberg Stiftung gGmbH.

7. REFERENCES

- [1] P. Jahankhani, V. Kodogiannis, and K. Revett, "EEG signal classification using wavelet feature extraction and neural networks," in *IEEE John Vincent Atanasoff 2006 International Symposium on Modern Computing, JVA'06*. IEEE, 2006, pp. 120–124.
- [2] J. Lin and L. Qu, "Feature extraction based on morlet wavelet and its application for mechanical fault diagnosis," *Journal of Sound and Vibration*, vol. 234, no. 1, pp. 135–148, 2000.
- [3] Y. Mallet, D. Coomans, J. Kautsky, and O. De Vel, "Classification using adaptive wavelets for feature extraction," *IEEE Trans. Pattern Analysis and Machine Intelligence*, vol. 19, no. 10, pp. 1058–1066, 1997.
- [4] J. Kovacevic and M. Vetterli, "Perfect reconstruction filter banks with rational sampling factors," *IEEE Trans. Signal Processing*, vol. 41, no. 6, pp. 2047–2066, 1993.
- [5] I. Bayram and I.W. Selesnick, "Frequency-domain design of overcomplete rational-dilation wavelet transforms," *IEEE Trans. Signal Processing*, vol. 57, no. 8, pp. 2957–2972, 2009.
- [6] T. Blu, "A new design algorithm for two-band orthonormal rational filter banks and orthonormal rational wavelets," *IEEE Trans. Signal Processing*, vol. 46, no. 6, pp. 1494–1504, 1998.
- [7] S.T.N. Nguyen and B.W.-H. Ng, "Bi-orthogonal rational discrete wavelet transform with multiple regularity orders and application experiments," *Signal Processing*, vol. 93, no. 11, pp. 3014 – 3026, 2013.
- [8] M. Vetterli, "Filter banks allowing perfect reconstruction," *Signal Processing*, vol. 10, no. 3, pp. 219–244, 1986.
- [9] T. Greiner, "Orthogonal and biorthogonal texture-matched wavelet filterbanks for hierarchical texture analysis," *Signal Processing*, vol. 54, no. 1, pp. 1–22, 1996.
- [10] Y. Wisutmethangoon and T. Q. Nguyen, "A method for design of Mth-band filters," *IEEE Trans. Signal Processing*, vol. 47, no. 6, pp. 1669–1678, 1999.
- [11] S. Werling, M. Mai, M. Heizmann, and J. Beyerer, "Inspection of specular and partially specular surfaces," *Metrology and Measurement Systems*, vol. 16, pp. 415–431, 2009.
- [12] T.-T. Le, M. Ziebarth, T. Greiner, and M. Heizmann, "Inspection of specular surfaces using optimized M-channel wavelets," in *Proceedings of the IEEE International Conference on Acoustics, Speech, and Signal Processing, ICASSP 2013*, Vancouver, Canada, May 2013.